Published in final edited form as:
J Magn Reson Imaging. 2011 February ; 33(2): 287–295. doi:10.1002/jmri.22437.

Whole Brain CBF Mapping using 3D Turbo Field Echo Imaging and Pulsed Arterial Tagging

Neville D. Gai, PhD[1], **S. Lalith Talagala, PhD**[2], and **John A. Butman, MD PhD**[1]

[1]Radiology and Imaging Sciences, Clinical Center, National Institutes of Health, Bethesda, MD

[2]NIH MRI Research Facility, National Institutes of Neurological Disorders & Stroke, National Institutes of Health, Bethesda, MD

Abstract

Purpose—To quantitate cerebral blood flow (CBF) in the entire brain using 3D EPI PULSAR (Pulsed STAR labeling) technique.

Materials and Methods—The PULSAR technique was modified to (a) incorporate a non-selective inversion pulse to suppress background signal (b) to use 3D echo planar (EPI) acquisition and (c) to modulate flip angle in such a manner as to minimize the blurring resulting from T1 modulation along the slice encoding direction. Computation of CBF was performed using the general kinetic model (GKM). In a series of healthy volunteers (n = 12), we first investigated the effects of introducing an inversion pulse on the measured value of CBF and on the temporal stability of the perfusion signal. Next, we investigated the effect of flip angle modulation on the spatial blurring of the perfusion signal. Finally, we evaluated the repeatability of the CBF measurements, including the influence of the measurement of arterial blood magnetization (a calibration factor for the GKM).

Results—The sequence provides sufficient perfusion signal to achieve whole brain coverage in about five minutes. Introduction of the inversion pulse for background suppression did not significantly affect computed CBF values, but did reduce the fluctuation in the perfusion signal. Flip angle modulation reduced blurring, resulting in higher estimates of GM CBF and lower estimates of WM CBF**.** The repeatability study showed that measurement of arterial blood signal did not result in significantly higher error in the perfusion measurement.

Conclusion—Improvements in acquisition and sequence preparation presented here allow for better quantification and localization of perfusion signal allowing for accurate whole brain CBF measurements in five minutes.

Keywords

Arterial spin labeling; 3D PULSAR; blurring reduction; whole brain perfusion imaging

INTRODUCTION

Arterial spin labeling (1) (ASL) provides non-invasive measurements of cerebral blood flow by using labeled blood as an endogenous contrast agent. Measurement of cerebral perfusion can provide unique information not achievable with other MRI contrasts in a number of clinical situations, e.g. differentiation of tumor recurrence from radiation necrosis. Clinically, bolus tracking of an exogenous gadolinium based contrast agent (GBCA) is

Corresponding Author: Neville Gai, PhD Radiology and Imaging Sciences (RAD&IS) 9000 Rockville Pike, Bldg 10/ Room 1C502X National Institutes of Health/ Clinical Center Bethesda, MD 20892 Phone: (301) 402-5114 Fax: (301) 496-9933 gaind@cc.nih.gov.

typically performed using dynamic susceptibility imaging. Use of tagged blood as contrast has several advantages as compared with techniques using exogenous dynamic contrast agents. Foremost of these is the elimination of risks associated with the administration of GBCA including anaphylaxis and nephrogenic systemic fibrosis. Expense and dose limitations also preclude multiple repetitions of the GBCA perfusion experiment.

Commercial implementations of ASL perfusion MRI are currently based on 2D multi-slice acquisitions. These sequences provide limited spatial coverage of the brain. Clinically there is a need for methods that provide whole brain coverage in a reasonable time, motivating the use of 3D acquisition.

Three dimensional acquisition has a number of potential benefits over 2D acquisition. In addition to permitting whole brain coverage and possibly higher SNR, 3D acquisition eliminates slice dependent variation of the perfusion signal resulting from slice dependent acquisition delay times in 2D acquisition. This is due to the fact that the SNR of 3D images is determined by the signal energy at the $(k_x, k_y, k_z) = 0$ point. The acquisition delay time can then be considered to be from the application of tagging or control pulses to the echo time of the acquisition through the center of k-space. Three dimensional acquisition of the imaging volume without gaps can also provide better reproducibility in longitudinal ASL based fMRI studies. For these reasons, a number of investigators have made use of 3D acquisition, either as segmented or single shot acquisitions. Examples of segmented 3D ASL techniques include the use of multi-shot spirals with pulsed arterial spin labeling (2) and with continuous arterial spin labeling (3). Single-shot techniques reduce variation in signal arising from phase inconsistencies in multi-shot techniques. 3D GRASE acquisition was implemented with FAIR pulsed arterial spin labeling (4) and with CASL (5). The use of single-shot 3D fast spin-echo spiral acquisitions has also been demonstrated (6). While fast spin-echo and GRASE acquisitions have the benefit of reducing T2* related artifacts that occur with gradient-echo EPI acquisitions, this comes at the expense of higher RF power deposition and prolonged acquisition times relative to pure EPI readouts. Talagala et al.(7) demonstrated the use of non-segmented 3D EPI with CASL in which a complete 3D data set was acquired using a train of z-phase encoded, low flip angle 3D EPI readouts following each CASL preparation interval. This approach referred to here as 3D Turbo Field Echo Planar Imaging (TFEPI) (turbo refers to the acquisition under non steady-state conditions) provides high k-space sampling efficiency. With centric encoded 3D TFEPI, true whole brain coverage using up to 35 slices with 4 mm slice thickness can be obtained. In addition, for high field imaging, SAR can be reduced by reducing the excitation angle used with 3D TFEPI while still maintaining sufficient SNR. Therefore, in this work, we further develop the use of 3D TEFPI for ASL perfusion imaging by combining it with the PULSAR technique (based on the EPISTAR technique (8)) described by Golay et al (9,10). Here we investigate modifications to the basic sequence to improve the temporal stability of the perfusion images, reduce blurring in 3D TFEPI images and improve quantitation and reproducibility of perfusion data.

Previously, it has been shown with 3D segmented acquisition FAIR (2) that use of inversion pulses results in superior temporal stability of perfusion images by reducing the background signal. Background suppression pulses have also been used in single shot 3D ASL studies (4-6). With 3D TFEPI, use of a centric-ordered acquisition can increase the effectiveness of background suppression pulses. However, use of multiple background suppression pulses can cause significant attenuation of the ASL signal (2,11) which can offset the advantages of background suppression. Accordingly, we employ a single non-selective inversion pulse (hyperbolic-secant pulse) to reduce temporal variability of the perfusion signal. Quantitative CBF values are compared with and without background suppression in gray matter and globally.

One potential complication with 3D TFEPI readout arises from the application of constant flip angles to acquire z-phase encodes under non-steady-state conditions. This results in blurring along z-axis due to modulation of k_z space, and hence, in errors in CBF values of gray matter and white matter. We analyze the effect of non-steady state constant flip angle imaging and correct for blurring by modulating the flip angle train such that magnetization in gray matter remains almost constant across all 3D-TFEPI shots.

To derive quantitative values, a general kinetic model (GKM) (12) is favored for pulsed arterial techniques due to its simplicity and ease of application. Application of the model requires (a) a well defined bolus of tagged blood and (b) complete delivery of the entire bolus to the voxel imaged at the time of measurement. In this work, a well defined bolus was obtained by incorporating a QUIPSS II saturation pulse (13) into the PULSAR sequence.

The most important measurement factor affecting CBF quantification with the GKM model is the equilibrium magnetization of the arterial blood signal. We therefore performed a repeatability study in order to quantify the error resulting from measurement of this factor.

MATERIALS AND METHODS

The original PULSAR sequence (9) was modified to include a QUIPSS II saturation pulse (13) and an inversion recovery (IR) pulse as shown schematically in Figure 1. The preparation scheme consists of a four pulse pre-saturation sequence to saturate magnetization in the imaging slab. This is followed by the labeling pulse which consists of one 180° adiabatic hyperbolic secant inversion pulse. For the case of the control sequence, two adiabatic inversion pulses with the same time duration and bandwidth as the labeling pulse are used. The amplitude of both inversion pulses for the control sequence is 2 lower than the labeling pulse. The labeling pulse inverts spins in the selected labeling slab (below the imaging slab) while the control pulse does not result in any net magnetization. However, the control pulse compensates for the magnetization transfer effect. Introduction of a QUIPSS II saturation pulse helps define bolus length and the non-selective IR pulse helps suppress the signal in GM, WM and CSF. This is followed by the imaging slab acquisition which consists of a train of low flip angle gradient echo planar imaging sequences with phase encoding along the z (slice) direction (7,14).We refer to the PULSAR sequence with 3D TFEPI acquisition (but no inversion pulse) as 3D PULSAR and that with the adiabatic inversion pulse is referred to as IR-3D-PULSAR.

Quantification of CBF was done using $f(\mathrm{TD})=\Delta M / [2\eta M_{0A}\tau \exp(-\mathrm{TD}/T_{1A})]$ (Eq. (2) in (12)), where ΔM is the perfusion signal, η is the inversion efficiency, M_{0A} is the equilibrium magnetization of arterial blood, τ is the duration of the bolus, TD is the delay between tagging and acquisition and T_{1A} is the T1 of arterial blood. T_{1A} is assumed to be 1650 ms at 3T (15). The inversion efficiency, η is assumed to be 0.91 (derived on a Philips 3T scanner (10)). For centric-ordered 3D acquisition, TD is defined by the time between the tagging inversion pulse and the $k_z = 0$ slice encoding which for our centric-ordered case corresponds to approximately the beginning of data acquisition. M_{0A} is difficult to measure directly as intracranial arteries are small and subject to partial volume errors. Therefore, we chose to measure M_{0V} directly from an ROI in the sagittal sinus and convert this to M_{0A} by correcting for the different transverse relaxation rates of arterial (R_{2A}^*) and venous (R_{2V}^*) blood by the equation $M_{0A} = M_{0V} \cdot \exp [\mathrm{TE} \cdot (R_{2V}^* - R_{2A}^*)]$. The relaxation rate of arterial blood, R_{2V}^*, was assumed to be 46.2 s^{-1} and $R_{2A}^* = 18.8\ s^{-1}$ at 3T (10).

Measurement of blood signal in the sagittal sinus is done on the first phase of the 3D-PULSAR image set to ensure that the signal in the sagittal sinus is free of any prepared (inversion or saturation) magnetization as the mean transit time through the vascular bed is

about 4 s (12) (much greater than the TD time of 1.8 s used here). A separate sequence, which in turn entails extra processing due to differences in image scaling, was therefore not required.

For the case when an IR pulse is used (IR-3D-PULSAR), an extra inversion efficiency factor is applied to M_{0A} (= $M_{0A} \cdot \eta$) derived from the first phase of the 3D-PULSAR images in addition to image scaling factors. For the IR-3D-PULSAR acquisition, ΔM was calculated as *(Label – Control)* instead of *(Control – Label)* images to account for the inversion pulse (2).

Background Suppression

A single inversion pulse was introduced with inversion time around 900 ms. In combination with the saturation of the imaging slab, this results in GM, WM and CSF longitudinal magnetization values of 0.25, 0.43 and 0.03 (based on published values for T1/T2) for centric encoded data acquisition at 1800 ms after labeling and for the repetition time employed during scanning. This is in contrast to corresponding values of 0.75, 0.88 and 0.33 when no inversion pulse is used. Consequently, background signal is suppressed in all three tissue types.

The acquired ΔM(t) images were analyzed for temporal stability of the perfusion signal by calculating $\langle \sigma(\Delta M(t)) \rangle / \langle \Delta M(t) \rangle$ globally for the whole brain (Glo) and for ROIs in grey matter (GM), white matter (WM), CSF. All ROIs and slices were matched for both sequences.

In addition, CBF estimates in gray matter were compared for the two sequences. Erosion and dilation (to remove skull) followed by automated segmentation based on Otsu's algorithm (16) available in Matlab® was applied to all CBF maps to separate regions of high perfusion (approximating gray matter-GM) from lower perfusion (approximating white matter-WM). Mean GM CBF value was determined by averaging values over all slices.

Correcting for blurring

Typically, 3D acquisition under non steady state conditions results in blurring. For ASL techniques, this reduces GM CBF and increases WM CBF values due to partial volume effects. In 3D-TFEPI, the longitudinal magnetization after each RF excitation pulse can be described by (17)

$$M_z[n] = E_1 \cdot \cos\alpha \cdot M_z[n-1] + (1 - E_1) \cdot M_z[0] \quad [1]$$

and the transverse magnetization after each RF pulse is

$$M_{xy}[n] = E_2^* \cdot \sin\alpha \cdot M_z[n-1], n=1, \ldots, L \quad [2]$$

where E_1=exp(−TR/T1), E_2^*=exp(−TE/T2*), α is the excitation angle and L is the total number of slice encodings. Use of a constant flip angle results in a decay of the transverse magnetization towards its final steady-state value. This signal modulation (which appears along slice phase encoding in 3D TFEPI acquisition) is the cause of the blurring. To correct for this modulation, the flip angles can be adjusted such that the magnetization stays approximately constant across all slice encodings. This is achieved if the flip angle is calculated as (17,18)

$$\alpha[n] = \sin^{-1}\{(\sin\alpha[0] \cdot \tan\alpha[n-1]) / (E_1 \cdot \sin\alpha[0] + (1 - E_1) \cdot \tan\alpha[n-1])\} \quad [3]$$

A particular final flip angle can be targeted and the flip angle schedule calculated within a few iterations (19). Figure 2A shows one such flip angle train calculated using gray matter T1/T2 values (1300 ms and 60 ms, respectively), TR/TE = 20/9 ms (corresponds approximately to TR/TE times used on the scanner), a final flip angle of 30° and with 31 slice encodings. (This corresponds to 24 slice acquisition with oversampling typically used with 3D acquisition.) Figure 2B shows the transverse magnetization for the constant flip angle (30°) case and for the modulated flip train. Magnetization remains mostly constant for the modulated flip angle train. The PSF of $M_{xy}(n)$ (Fig. 2C) clearly shows that increased blurring results from using the constant flip angle train. Figure 2D shows the effect of the PSF on a slice of thickness 4 mm. Constant flip angle scheme results in increased smearing of the signal along the slice direction. The peak signal (normalized to the ideal signal) is just 0.52 while it is 0.98 with the variable flip angle scheme. Simulations show that transverse magnetization (and hence SNR) increases with increasing final flip angle. However, increasing the final flip angle from 30° to 90° results in a mere 3% increase in magnetization at the center of k-space. In addition, on our scanner, increasing the final flip angle results in increasing values for TE/TR of the single-shot EPI acquisition due to RF pulse stretching. As a result, a final flip angle of 30° was used with variable flip angle excitation and for 31 slice encodings.

Repeatability Study

The derived CBF values follow an inverse relationship with arterial blood signal (M_{0A}). As described earlier, measurement for M_{0A} is typically done in a voxel in the sagittal sinus that is completely filled with blood and free of partial volume effects. Measurement of M_{0A} is considered to be an important source of error in CBF determination using GKM with a bolus cutoff pulse. We investigated the repeatability of CBF values across volunteers with and without this potential source of error (20).

For this purpose, four 3D PULSAR and four IR-3D-PULSAR scans were performed on each volunteer in the same session. M_{0A} was derived from signal measured in the sagittal sinus for each 3D PULSAR scan. GM CBF values were calculated for each case using the corresponding measured M_{0A} value. CBF values were also calculated for the four scans using an average value for M_{0A} to reflect other (pulse imperfections, differences in transit delay etc) errors. Since introduction of an IR pulse alters signal in the sagittal sinus**,** the average value of M_{0A} (denoted $\langle M_{0A} \rangle$) from the 3D PULSAR scan was used for CBF calculation for IR-3D-PULSAR. While CBF values obtained from 3D-PULSAR scans reflect variation mainly due to M_{0A}, values obtained using $\langle M_{0A} \rangle$ reflect other errors. The mean and standard deviation (σ) across four repeated scans was calculated for 3D-PULSAR and IR-3D-PULSAR. In addition, the various scans were repeated on two volunteers on two different days to assess reproducibility.

Imaging Protocol

All scans were performed on a Philips 3T Achieva scanner equipped with QUASAR dual mode gradients capable of maximum gradient amplitude of 80 mT/m and a slew rate of 200 T/m/s. A six channel receive-only head coil was used for acquisition. Scan parameters were: TR/TD=2380/1800 ms; 60 pairs of control/label images; tagging region width = 200 mm applied 20 mm inferior to imaging slab; data acquisition: 3D-TFEPI with 24 slices (31 slice encodings), fat suppression, 4 mm slice thickness, 80×80 matrix, SENSE factor=2.5 along phase encoding direction; DAC window ≈ 600ms; bolus duration τ = 900 ms; scan time ≈ 5 min. The excitation pulses were Gaussian filtered sinc of duration 1.14 ms. Fat suppression was achieved by applying a pulse of duration 7.5 ms at off-resonance. Fat suppression pulse was employed once prior to acquisition of each 3D data set. For IR-3D-PULSAR, the TI

time was fixed at 920 ms prior to data acquisition. The manufacturer supplied CLEAR option was used to correct for receive field inhomogeneity for all images.

A total of twelve healthy volunteers were scanned under an IRB approved protocol. Informed consent was obtained from all volunteers after the nature of the procedure had been fully explained. Of the twelve volunteers, five were used for the background suppression study and the repeatability study; a different set of five volunteers were used only for the blurring reduction study; one was used only for the repeatability study only while one was used for repeatability across different days along with another subject from the first group.

RESULTS

Quantification with and without background suppression

Table 1 shows the values for $\langle\sigma(\Delta M(t))\rangle$ / $\langle\Delta M(t)\rangle$ averaged over all five volunteers. Note that $\Delta M(t)$ value in CSF is small, resulting in higher ratios of $\langle\sigma(\Delta M(t))\rangle$ / $\langle\Delta M(t)\rangle$. A considerable reduction in this measure for GM, WM and whole brain perfusion signal with IR-3D-PULSAR as compared to 3D-PULSAR is seen indicating better temporal stability. In addition, mean signal within CSF space was just 0.29±0.76 with the background suppression inversion pulse as opposed to −0.93±1.76 indicating better suppression of spurious perfusion signal in CSF.

Figure 3 shows CBF maps (in ml/100g/min) for every fourth slice of the 24 slices acquired with 3D-PULSAR and the corresponding images with IR-3D-PULSAR. Figure 4 shows a plot of the GM CBF values obtained with the two sequences. The average GM CBF value across the five volunteers was 58.2 ml/100g/min with 3D-PULSAR and 58.9 ml/100g/min with IR-3D-PULSAR. Note that good correspondence between the two values indicates that the assumed value for inversion efficiency ($\eta = 0.91$) is accurate.

Blurring reduction

Figure 5 shows six transverse CBF image slices (out of 24) and reformatted sagittal and coronal slices obtained using the two different scans: constant flip angle (A, C) and modulated flip angle (B, D). As can be seen, CBF images obtained with the modulated excitation angle train appear sharper and suffer from lower partial volume effects. This is also reflected in the GM CBF values reported in Table 2. Mean value for GM CBF was 55.8±8.4 and 65.9±5.7 ml/100 g/min for the five volunteers before and after correction for blurring. There was a corresponding reduction in mean WM CBF values from 10.1±2.4 to 8.0±1.8 ml/100 g/min indicating reduced partial volume effects after correction. A paired t-test between the CBF values shows significant differences ($p<0.05$) for both gray and white matter before and after blurring correction. The number of voxels classified as gray matter was also lower for the modulated flip angle case by an average of 20% indicating reduced blurring.

Repeatability data

Table 3 shows mean and standard deviation (σ) values across repeated scans for the globally averaged GM segmented images for the two cases: 3D-PULSAR and IR-3D-PULSAR. Figure 6 shows three select segmented GM CBF image slices from the 3D stack (row A) obtained with IR-3D-PULSAR; standard deviation images across four repeated scans for 3D-PULSAR (B) and (C) standard deviation images for IR-3D-PULSAR. (Window/level for images in (B) and (C) is the same but different from images in (A).) Images obtained with $\langle M_{0A}\rangle$ for 3D-PULSAR show a similar qualitative appearance as images in Figure 6B indicating that the increased noise is not related to use of measured M_{0A}s vs $\langle M_{0A}\rangle$.

Average σ across six volunteers is 3.93 when using individually measured M_{0A}s but is 3.15 with use of $\langle M_{0A} \rangle$ for 3D-PULSAR while it is just 2.51 for IR-3D-PULSAR. Average GM CBF values were within 3% for two volunteers across two different scanning sessions.

DISCUSSION

Our objective was to perform whole brain perfusion imaging in a clinically reasonable scan time of about five minutes. Pulsed arterial tagging along with 3D turbo field echo planar acquisition allows for sufficient SNR to achieve this goal. Although the data presented in this work was from 24 slice acquisitions, we have used the sequence provided here to acquire up to 32 slices of 4 mm thickness with an in-plane resolution of 2.9×2.9 mm in other ongoing studies. Use of an inversion pulse reduced temporal fluctuations in GM and WM and suppressed spurious signal from the CSF. It also showed improvement in CBF maps in areas of high susceptibility as seen in Figure 3. A shorter TR is possible even with a background suppression pulse since a saturation pulse is applied to the imaging slab at the beginning of the spin labeling sequence. Extended data acquisition in the non-steady state can result in substantial blurring and result in reduced values for GM CBF as well as misclassification of gray matter CBF. Using a modulated flip angle train to account for this blurring gives higher values in GM by reducing partial volume effects.

The acquisition scheme used here (3D TFEPI) has advantages and disadvantages compared to 3D GRASE or spiral acquisition schemes. While single-shot spiral scanning (3D FSE stack of spirals) (6) can achieve a similar spatial coverage and resolution as the 3D TFEPI scheme, perfusion images will show increased off-resonance related blurring. Spiral imaging is sensitive to gradient group delays which can result in artifacts particularly when scanning at oblique angles. Compared to 3D TFEPI, 3D GRASE can offer improved off-resonance response. However, since 3D TFEPI uses low flip angle excitation pulses and 3D GRASE depends on large flip angle excitation and refocusing pulses, the sampling efficiency in 3D TFEPI can be higher than that of 3D GRASE when selective pulses are used. This will to some extent improve the spatial resolution and/or coverage along the slice encoding direction. However, based on a different pulse design (for example, by using non-selective refocusing pulses), it may be possible to make a 3D GRASE acquisition faster than a 3D TFEPI acquisition. By keeping echo times relatively short (TE ~ 9 ms) with our TFEPI acquisition, the susceptibility effects are considerably reduced.

Values for bolus length and transit time were fixed based on empirical observations of the perfusion signal to allow sufficient signal to noise as well as to fulfill assumptions related to the general kinetic model. A bolus cut-off time of 900 ms ensures that even the fastest spins in the external carotid arteries (~ 100 cm/s) have not yet completely left the tagging slab. Uncertainty in transit times can cause errors in the perfusion values. Using longer delay times can reduce the magnitude of these errors at least for GM CBF. We eschewed the use of vascular signal crushers since the reduction in perfusion signal was considerable and the use of a sufficiently long delay time (1.8 s) didn’t warrant it. In patients with severely compromised flow, this will lead to increased vascular signal despite the prolonged delay time. Areas with prolonged arrival times will show reduced CBF values. White matter perfusion values are generally unreliable with pulsed arterial sequences due to longer transit times. This violates the GKM model condition which requires that the entire bolus reach the imaging voxel under consideration. In addition, partial volume effects result in additional errors (21). Another recent study (22) has shown that about 45% of WM pixels show no statistically significant perfusion signal in a clinically feasible scan time of five minutes. Consistent with other studies dealing with pulsed arterial labeling, we found increased variability and decreased values for white matter CBF (21,23). As a result, except to show reduction in blurring, WM CBF values should not be taken as accurate.

A possible explanation of higher WM values reported in some other papers using pulsed labeling with similar or smaller bolus time could be contamination of perfusion signal from adjoining higher perfusion GM areas. Reducing the duration of the bolus while keeping delay time the same would result in an increase in the allowed bolus transit time and improve white matter CBF values. In addition, reducing the bolus duration may reduce errors resulting from dispersion of the bolus. Reducing bolus duration would however impact the SNR of the perfusion signal and entail prolonged scan times. Increased bolus duration can also result in reduced perfusion values due to dispersion of the bolus. Typically, the effect is much less with the QUIPSS II like sequence used here (24). Use of multiple inversion times (25) or a Look-Locker acquisition along with a model free approach (10) can address the issue of different arrival times. Such an approach would compromise SNR, resolution and spatial coverage and would therefore be more useful for CBF quantification in a few slices with 2D acquisition. Patients with severely compromised perfusion may still not be accurately quantified by the above methods.

We showed that as long as partial volume and saturation effects are avoided, M_{0A} measurement does not significantly alter results when compared with other sources of error. Standard deviation maps for 3D-PULSAR reflect errors due to measurement of M_{0A} as well as errors due to relatively poorer background suppression. M_{0A} measurement errors result in a standard deviation that is higher than when M_{0A} variation is absent (as when $\langle M_{0A} \rangle$ is used with 3D-PULSAR). The average coefficient of variation (COV) defined as (σ / μ) is higher by about 19.8%. The fact that the σ map for 3D-PULSAR is more heterogeneous when compared with the IR-3D-PULSAR maps, particularly adjacent to CSF spaces, reflects the superior background suppression of IR-PULSAR; COV is further reduced by about 21% with IR-3D-PULSAR over 3D-PULSAR using $\langle M_{0A} \rangle$. However, performing the Student t-test reveals no significant difference between values obtained using individual M_{0A} or $\langle M_{0A} \rangle$ (t-value=1.14<2.23 for a p-value of 0.05) for 3D-PULSAR indicating that M_{0A} measurements do not change results significantly.

Gray matter CBF values were obtained by segmenting out regions of high perfusion from those that exhibit lower perfusion. This has some limitations and can result in cross-contamination of signal from WM and GM. A gray matter map could be independently derived from a higher resolution scan and applied to the CBF map to determine perfusion signal originating in the GM after registration and correction for any motion between the two scans.

Despite the use of CLEAR to correct for receive field inhomogeneity, shading effects were seen in certain acquired data sets, a result of uncorrected transmit and receive field inhomogeneity. Correction for residual RF field inhomogeneity should mitigate the shading effect and result in improved perfusion images.

In conclusion, modifications to the PULSAR sequence permit whole brain CBF measurements to be performed in an efficient manner. Further improvements in accuracy and efficiency are possible and are areas of future exploration. For example, multi-transmit body coils can reduce errors introduced by B1 inhomogeneity. Improvements in coil design and parallel imaging algorithms can further reduce acquisition and echo time with subsequent reduction in EPI related susceptibility effects. Scanning at higher fields (7T) can compensate for shorter acquisition time related SNR reduction.

Acknowledgments

The authors thank Dr. Xavier Golay, Esben Petersen, Maarten Versluis and Dr. Frank Hoogenraad for initial help provided for the project.

This work was supported by the Intramural Research Program of NIH.

REFERENCES

1. Williams DS, Detre JA, Leigh JS, Koretsky AP. Magnetic resonance imaging of perfusion using spin inversion of arterial water. Proc Natl Acad Sci U S A. 1992; 89(1):212–216. [PubMed: 1729691]
2. Ye FQ, Frank JA, Weinberger DR, McLaughlin AC. Noise reduction in 3D perfusion imaging by attenuating the static signal in arterial spin tagging (ASSIST). Magn Reson Med. 2000; 44(1):92–100. [PubMed: 10893526]
3. Talagala SL, Ye FQ, Ledden PJ, Chesnick S. Whole-brain 3D perfusion MRI at 3.0 T using CASL with a separate labeling coil. Magn Reson Med. 2004; 52(1):131–140. [PubMed: 15236376]
4. Gunther M, Oshio K, Feinberg DA. Single-shot 3D imaging techniques improve arterial spin labeling perfusion measurements. Magn Reson Med. 2005; 54(2):491–498. [PubMed: 16032686]
5. Fernandez-Seara MA, Wang Z, Wang J, et al. Continuous arterial spin labeling perfusion measurements using single shot 3D GRASE at 3 T. Magn Reson Med. 2005; 54(5):1241–1247. [PubMed: 16193469]
6. Duhamel, G.; Alsop, DC. Single-shot susceptibility insensitive whole brain 3D fMRI with ASL. Proceedings of the 12th Annual Meeting of ISMRM; Kyoto. 2004; (abstract 518)
7. Talagala, SL.; Slavin, GS.; Ostuni, J.; Chesnick, S. CASL Perfusion MRI with Non-segmented Low Flip Angle 3D EPI. Proceedings of the 14th Annual Meeting of the Society of Magnetic Resonance; Seattle. 2006; (abstract 3422)
8. Edelman RR, Chen Q. EPISTAR MRI: multislice mapping of cerebral blood flow. Magn Reson Med. 1998; 40(6):800–805. [PubMed: 9840822]
9. Golay X, Petersen ET, Hui F. Pulsed star labeling of arterial regions (PULSAR): a robust regional perfusion technique for high field imaging. Magn Reson Med. 2005; 53(1):15–21. [PubMed: 15690497]
10. Petersen ET, Lim T, Golay X. Model-free arterial spin labeling quantification approach for perfusion MRI. Magn Reson Med. 2006; 55(2):219–232. [PubMed: 16416430]
11. Garcia DM, Duhamel G, Alsop DC. Efficiency of inversion pulses for background suppressed arterial spin labeling. Magn Reson Med. 2005; 54(2):366–372. [PubMed: 16032674]
12. Buxton RB. Quantifying CBF with arterial spin labeling. J Magn Reson Imaging. 2005; 22(6):723–726. [PubMed: 16261574]
13. Wong EC, Buxton RB, Frank LR. Implementation of quantitative perfusion imaging techniques for functional brain mapping using pulsed arterial spin labeling. NMR Biomed. 1997; 10(4-5):237–249. [PubMed: 9430354]
14. Gai, ND.; Talagala, SL.; Golay, X.; Hoogenraad, FG.; Butman, JA. Evaluation of 3D EPI PULSAR with and without Background Suppression Inversion Recovery Pulse. Proceedings of the 15th Annual Meeting of the Society of Magnetic Resonance; Berlin. 2007; (abstract 3486)
15. Lu H, Clingman C, Golay X, van Zijl PC. Determining the longitudinal relaxation time (T1) of blood at 3.0 Tesla. Magn Reson Med. 2004; 52(3):679–682. [PubMed: 15334591]
16. Otsu N. A threshold selection method from gray level histograms. IEEE Trans Syst, Man, Cyber. 1979; 9:62–66.
17. Haacke, EM.; Brown, RW.; Thompson, MR.; Venkatesan, R. Magnetic resonance imaging : physical principles and sequence design. Wiley; New York: 1999. p. 454-464.
18. Stehling MK. Improved signal in “snapshot” FLASH by variable flip angles. Magn Reson Imaging. 1992; 10(1):165–167. [PubMed: 1545677]
19. Gai, N.; Talagala, SL.; Butman, J. Accurate gray matter CBF mapping in whole brain IR 3D PULSAR imaging through flip angle modulation. Proceedings of the 17th Annual Meeting of ISMRM; Honolulu. 2009; (abstract 3648)
20. Gai, N.; Talagala, SL.; Butman, J. Effect of arterial blood signal measurements on the repeatability and accuracy of whole brain CBF values with 3D-PULSAR Imaging. Proceedings of the 18th Annual Meeting of ISMRM; Stockholm. 2010; (abstract 4076)

21. van Gelderen P, de Zwart JA, Duyn JH. Pittfalls of MRI measurement of white matter perfusion based on arterial spin labeling. Magn Reson Med. 2008; 59(4):788–795. [PubMed: 18383289]

22. van Osch MJ, Teeuwisse WM, van Walderveen MA, Hendrikse J, Kies DA, van Buchem MA. Can arterial spin labeling detect white matter perfusion signal? Magn Reson Med. 2009; 62(1):165–173. [PubMed: 19365865]

23. Ye FQ, Berman KF, Ellmore T, et al. H(2)(15)O PET validation of steady-state arterial spin tagging cerebral blood flow measurements in humans. Magn Reson Med. 2000; 44(3):450–456. [PubMed: 10975898]

24. Petersen, ET.; Golay, X. The effect of bolus length and dispersion on arterial spin labeling (ASL) flow quantification. Proceedings of the 18th Annual Meeting of ISMRM; Stockholm. 2010; (abstract 514)

25. Hendrikse J, van Osch MJ, Rutgers DR, et al. Internal carotid artery occlusion assessed at pulsed arterial spin-labeling perfusion MR imaging at multiple delay times. Radiology. 2004; 233(3): 899–904. [PubMed: 15486211]

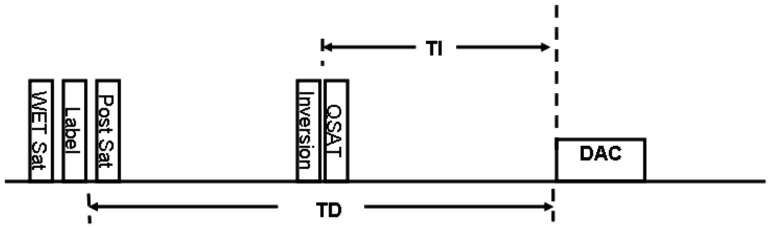

Figure 1.
Schematic representation of the 3D-IR-PULSAR sequence. The saturation pulse provides bolus definition while the inversion pulse improves background suppression and leads to reduced perfusion signal fluctuation. DAC denotes the data acquisition window which uses 3D TFEPI acquisition.

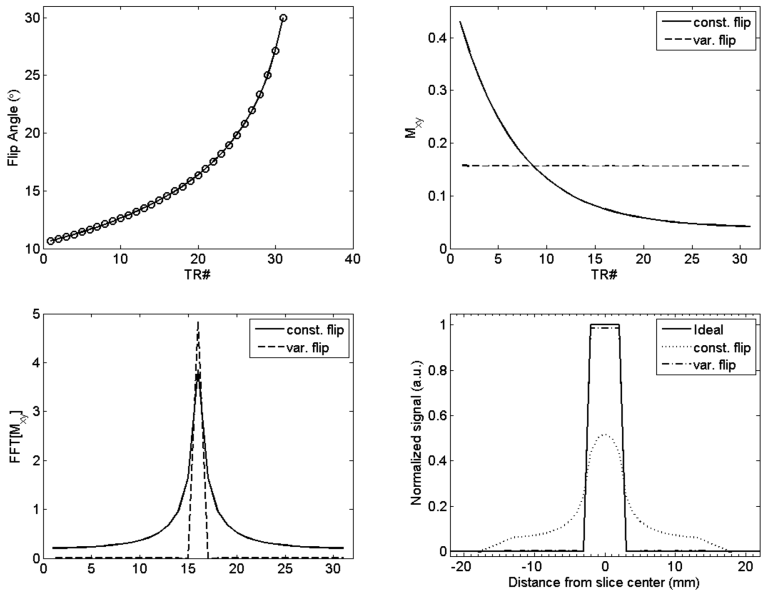

Figure 2.

Simulations depicting source of blurring and correction scheme (A) Variable flip angles used with 3D TFEPI acquisition with maximum flip angle of 30° (top-l) (B) transverse magnetization with constant flip angle scheme and with the modulated flip angle scheme (top-r) (C) PSF for the constant and variable flip angle schemes (bottom-l) and (D) the effect of the PSF on the slice profile (bottom-r). Center slice of thickness 4 mm is considered. Constant flip angle scheme results in increased dispersion of the magnetization signal into neighboring slices while variable flip angle scheme provides an almost ideal slice profile.

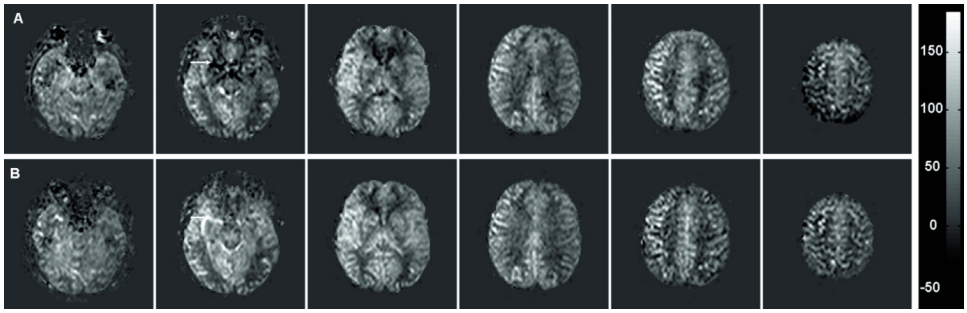

Figure 3.
CBF maps obtained with (A) 3D-PULSAR and (B) IR-3D-PULSAR. Every fourth slice from a 24 slice acquisition is shown. Scale on the right is in ml/100g/min.

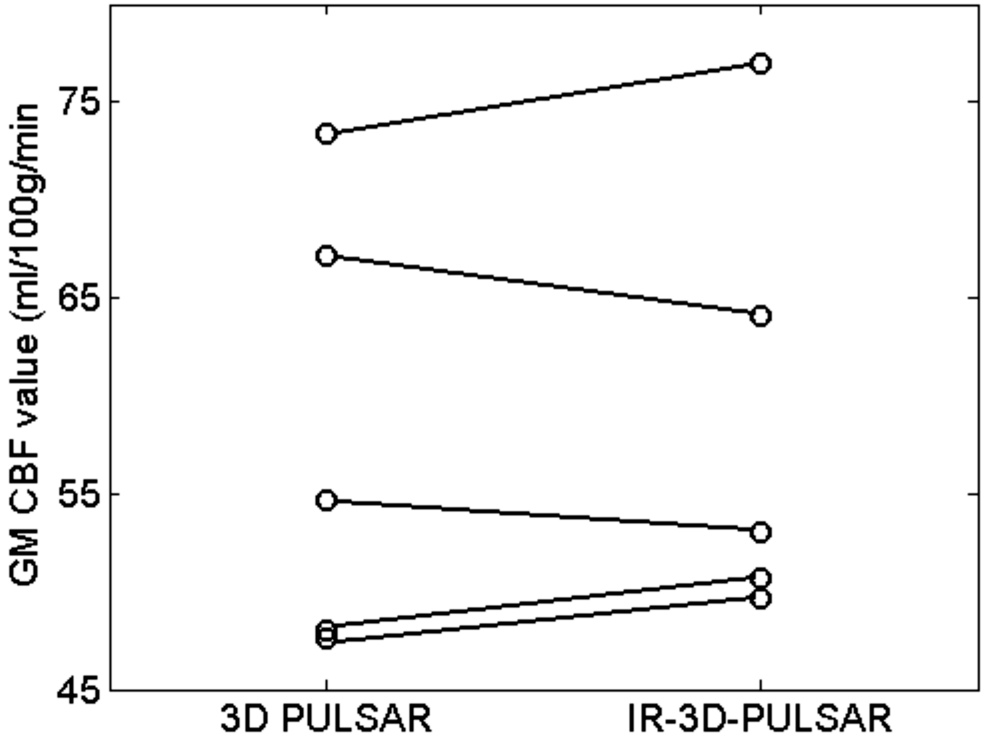

Figure 4.

Plot shows gray matter perfusion values for five volunteers with and without background suppression pulse. Average GM perfusion across volunteers is 58.2 ml/100g/min for 3D PULSAR and 58.9 ml/100g/min for IR-PULSAR case. Good correspondence between the two (3D PULSAR and 3D-IR-PULSAR) values for each volunteer is seen.

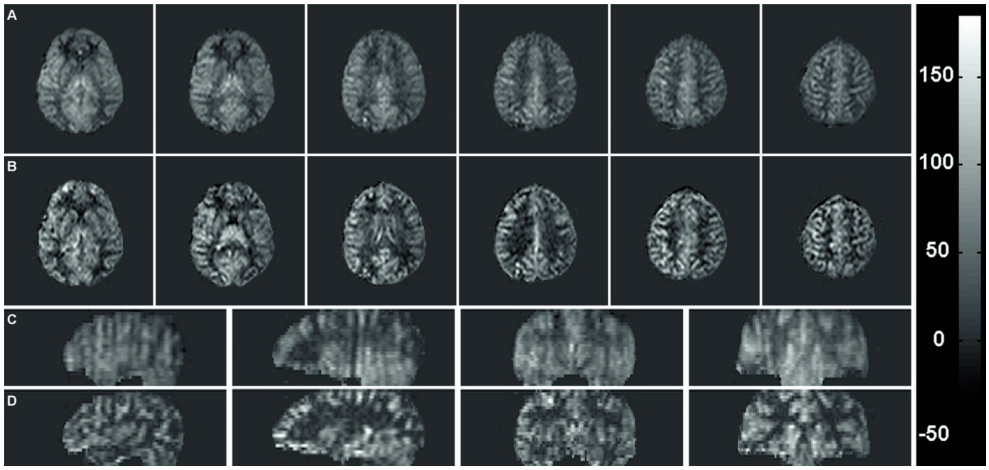

Figure 5.
Correction for blurring shows improved localization of the perfusion signal. Six transverse slices and reformatted sagittal and coronal slices obtained with (A, C) constant flip angle and (B, D) modulated flip angle are shown. Scale on right is in ml/100g/min and window/level is the same for all images.

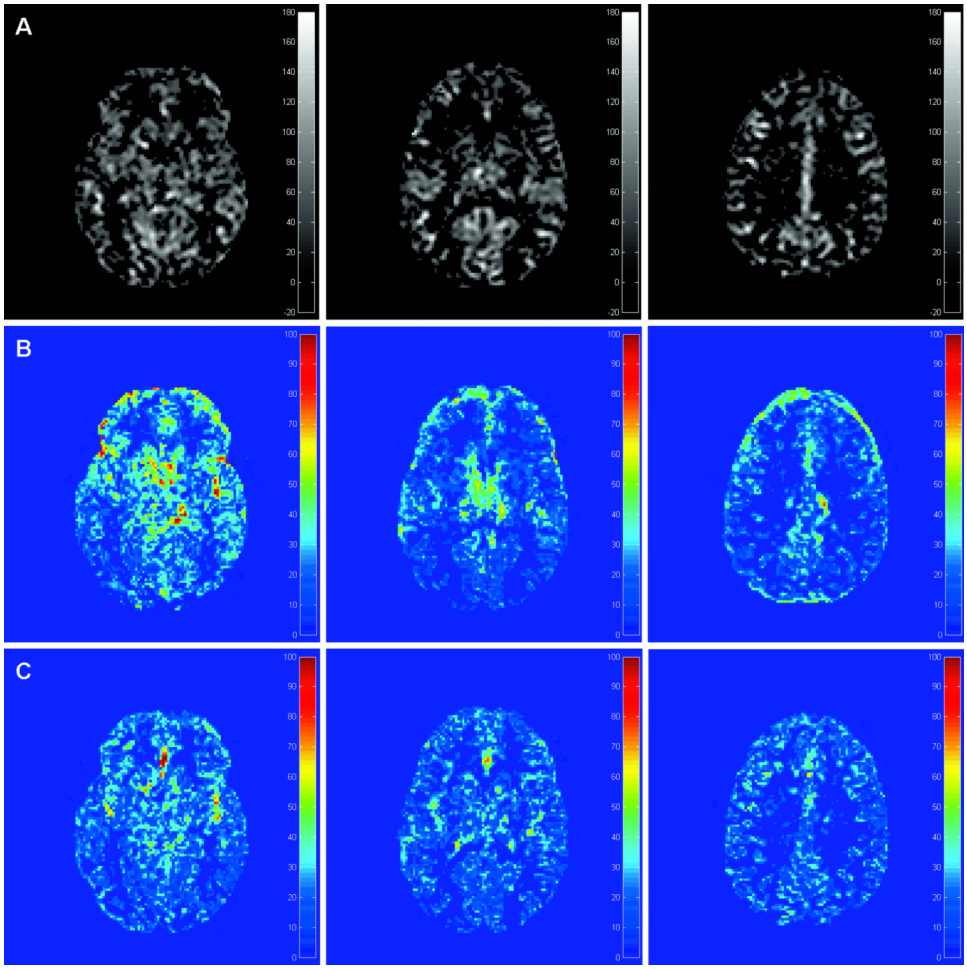

Figure 6.
Standard deviation maps obtained with repeatability study. Top row (A) shows the segmented GM CBF map for three slices while (B) shows the σ map across four repeated scans with 3D-PULSAR and (C) shows the σ map with IR-3D-PULSAR. Notice the poorer reproducibility of perfusion signal in areas close to CSF with 3D-PULSAR due to increased background noise.

Table 1

Perfusion signal stability (measured using $\langle\sigma(\Delta M)\rangle/\langle\Delta M\rangle$) in gray matter, white matter, CSF and globally with 3D-PULSAR and IR-3D-PULSAR.

	3D PULSAR	3D-IR-PULSAR
$\langle\sigma(\Delta M_{GM})\rangle/\langle\Delta M_{GM}\rangle$	1.53±0.87	1.13±0.43
$\langle\sigma(\Delta M_{WM})\rangle/\langle\Delta M_{WM}\rangle$	4.4±2.72	2.43±1.5
$\langle\sigma(\Delta M_{CSF})\rangle/\langle\Delta M_{CSF}\rangle$	−7.12±9.28*	11.67±40*
$\langle\sigma(\Delta M_{Glo})\rangle/\langle\Delta M_{Glo}\rangle$	0.31±0.03	0.14±0.04

*Mean values for CSF perfusion signal are very low resulting in large and/or negative values for $\langle\sigma(\Delta M_{CSF})\rangle/\langle\Delta M_{CSF}\rangle$.

Table 2

GM CBF values obtained from constant flip angle acquisition (which results in blurring) and from variable flip angle acquisition (reduced blurring). The increase in values is due to better localization of the perfusion signal. Values are in ml/100g/min.

Volunteer	Constant Flip		Variable Flip	
	GM CBF	*WM CBF*	*GM CBF*	*WM CBF*
1	69.0	12.5	77.3	9.0
2	51.6	12.6	63.0	10.2
2	55.8	8.8	62.6	7.6
3	59.1	9.7	62.9	7.7
5	51.5	7.0	58.2	5.5

Table 3

Repeatability study with the two sequences for six volunteers. Shown are the mean and standard deviation values across four repeat scans. Values are in ml/100g/min.

Volunteer	3D PULSAR	IR-3D-PULSAR
1	57±3.4	59±3.9
2	53±5.6	54±0.9
3	64±2.4	62±1.3
4	58±3.0	61±2.2
5	59±4.9	56±2.6
6	71±4.3	73±4.2